RSC Advances




ROYAL SOCIETY OF CHEMISTRY

www.rsc.org/advances

Journal Name

RSCPublishing

ARTICLE

# Enhanced electrochemical performances of $FeO_x$/graphene nanocomposites as anode materials for alkaline nickel-iron battery

Cite this: DOI: 10.1039/x0xx00000x

Received 00th January 2012,
Accepted 00th January 2012

DOI: 10.1039/x0xx00000x

www.rsc.org/

Wei Jiang [a d], Fei Liang [a b], Jianwei Wang [a d], Lei Su [a c], Yaoming Wu* [a b] and Limin Wang* [a b]

A new type of graphene-based $FeO_x$ nanocomposites has been synthesized by high temperature solid-state reaction using $FeC_2O_4 \cdot 2H_2O$. The synthesis conditions are optimized by thermogravimetric analysis of the precursor. When evaluated as anode material for alkaline nickel-iron battery, the $FeO_x$/graphene nanocomposites deliver a high specific capacity of 552.1 mAh $g^{-1}$ at current density of 200 mA $g^{-1}$ and remain 91% of the initial capacity after 100 cycles. Furthermore, the hybridized $FeO_x$/graphene materials only provide 26% capacity decay when the discharge current density converts from 200 mA $g^{-1}$ to 1000 mA $g^{-1}$. The enhanced cycling and high-rate performance is owing to the high specific surface area of iron oxide nanoparticles and particular electric conductivity of graphene. This study suggests a safe, inexpensive and powerful rechargeable iron electrode, enabling the promising prospect of large-scale energy storage based on the aqueous iron-based rechargeable battery.

## 1. Introduction

Rechargeable batteries are extraordinary suitable for large-scale storage of electrical energy based on their high energy efficiency and scalability[1-3]. As an example, Lithium ion battery, lead-acid battery and nickel-metal hydride (Ni-MH) battery have played major roles in various application fields, respectively. Meanwhile, the relatively low cost, eco-friendliness as well as the further safety requirements for rechargeable batteries have also attracted increasingly attention. The unreliable safety of lithium ion battery lies in the organic electrolytes and the high activity of Li containing in electrode materials[4-6] has been questioned by most of the researchers. More than that, the toxicity of lead-acid battery and the high cost limitation of Ni-MH battery are seemly irreversible. Consequently, searching for promising alternatives which could be applied with inexpensive materials in relatively safe aqueous electrolytes is extremely urgent.

Developed around 1900s by Waldemar Jungner and Thomas Edison, nickel-iron battery used to be widely discussed for large-scale energy storage[7-9]. With $Ni(OH)_2$ as the cathode and iron as the anode, the century-old Ni-Fe battery was considered to be one of the most promising secondary batteries for a long time[9]. Nowadays, the Ni-Fe energy storage systems have been widely employed into the electricity grid owing to their low cost, durable in use, eco-friendliness and safety. Nevertheless, the high self-discharge[10], relative low energy efficiency[11, 12], especially the low power density[13] of the iron anode in aqueous alkaline media are the principal drawbacks seriously restricting further utilization of iron battery. Because of the passivation[14, 15] onto the surface of iron electrode, the practical capacity only achieves as low as nearly 1/3 of the theoretical value (962 mAh $g^{-1}$). Seriously, the formation of passive layer also leads to the bad performance in high-rate discharge. It is worthwhile to significantly improve the electrochemical performances of iron electrode at high discharge rate, aimed at applications in hybrid electric vehicles (HEV) and electric vehicles (EV) where high current response is needed.

Graphene-based composites have been intensively explored in a wide range of applications[16,17], including supercapacitors[18], fuel cells[19], photovoltaic devices[20], photocatalysis[21], batteries[22-26], and so on. In the previous study, Wang[27] reported a strongly coupled $FeO_x$/graphene hybrid as anode for ultrafast nickel-iron battery, they successfully increased the charging and discharging rates by nealy 1000-fold over traditional Ni-Fe batteries. In this work, a novel hybridized $FeO_x$/graphene anode material was prepared through a relatively simple high temperature solid-state reaction process instead of hydrothermal synthesis. The iron oxide particles recrystallized on the reduced graphene sheets during high temperature decomposition process. Obviously, direct growth of iron nanoparticles on graphene sheets provided a good contact between the $FeO_x$ nanoparticle and the two-dimensional network of graphene, thus realized efficient conduction of charge carriers and enhances the structural stability. Consequently, the $FeO_x$/graphene composites can afford excellent electrochemical performances at high discharge current density.

## 2. Experimental Section

### 2.1 Synthesis of the hybridized $FeO_x$/graphene materials

Graphene oxide (GO) was made by a modified Hummers method[28] using graphite powder (200 mesh, 99.9999%, Sigma-Aldrich). The $FeO_x$/graphene hybrids were synthesized by a ball milling method followed by high temperature solid-state reaction process. Ferrous oxalate dihydrate (99.99%, Sigma-Aldrich) (FOD) and the as-prepared GO (10 mg/mL) were mixed based on the mass ratio ($m_{FOD}$:$m_{GO}$ = 100:1.0, 100:1.5 and 100:2.0 ), and 5% glucose was added to provide the reducing agent, and ethanol (5 mL) was used as the dispersing agent. Then the raw materials were ball-milled respectively under Ar atmosphere using a spex800 ball mill machine for 6 h with the ball-to-powder weight of 10:1. The intermediate products were kept at 80℃ for 12 h to intensive drying under vacuum. After that, the obtained precursors were heated at 350℃ for 0.5 h, then, 400℃ for 6 h, and finally, calcinated at 700℃ for 16 h under argon atmosphere to produce the final $FeO_x$/graphene composites. For comparison, $FeO_x$ composites were also prepared by a similar procedure in the absence of GO.

### 2.2 Characterization

Thermogravimetric analysis of the $FeO_x$/graphene precursor was investigated using a TG/DSC (SDT-2960, USA) apparatus with a temperature range from 100℃ to 700℃ (10℃ $min^{-1}$) under argon atmosphere. Furthermore, the composition and phase purity of the as-prepared samples were characterized by X-ray diffraction (XRD) (D8 Focus, Bruker, Germany). SEM images were carried out on an S-4800 (Hitachi, Japan) scanning electron microscopy (SEM). Transmission electron microscopy (TEM) and high-resolution TEM (HRTEM) images were carried out on a Hitachi-600 transmission electron microscope at an acceleration voltage of 200 kV. X-ray photoelectron spectroscopy (XPS) measurement was performed on a ESCALAB MK Ⅱ XPS Spectrometer to analyze the surface composition, using monochromated Al Kα X-rays. Cyclic voltammetry (CV) measurements were performed using a VMP3 Electrochemical Workstation (Bio-logic Inc.) in the range of -0.4 V to -1.4 V on a three-electrode configuration, where a mercury/mercuric oxide (MMO) was used as the reference electrode ($E^0$ = +0.098 V vs. the normal hydrogen electrode), and nickel hydroxide as the counter electrode. Particularly, the electrolyte was 8 M KOH and 1 M LiOH mixed aqueous solution.

### 2.3 Preparation of working electrodes and electrochemical measurements

The anode electrode typically contained 92 wt% of the synthesized $FeO_x$/graphene materials, 5 wt% of bismuth oxide, and 3 wt% of hydroxypropyl methyl cellulose (HPMC). After the mixture was dispersed in D.I. water, the pastes were then loaded onto a circular Ni foam current collectors (r = 8 mm, 110 ppi). The substrates were dried at 80℃ for 6 h in vacuum and then compressed to 0.5 mm thickness before measurement. Subsequently, the working electrodes were tested in a miniature cell, using two sintered nickel electrodes as cathode to achieve excess capacity and no-woven PP cloth as separator. According to the related references[29], we chosed 8 M KOH aqueous solution including 1 M LiOH as the electrolyte. Finally, the electrochemical measurements were carried out by a LAND battery-test instrument (Wuhan, China) at room temperature. The specific capacity and cycle life at different current densities were tested to evaluate the performance of the hybridized materials.

## 3. Results and discussion

TG-DSC analysis (Fig. 1) of the ball-milled precursor was carried out to investigate the solid-phase reaction process of $FeO_x$/graphene precursor within the temperature range 100℃ to 700℃ at a rate of 10℃ $min^{-1}$. The results indicate three significant weight loss regions. The first region (150-200℃) is related to the dehydration of the hydrates. The second platform of weak weight loss is observed at approximate 330 ℃, corresponding to the GO reduction process based on the weight loss ratio. Subsequently, the thermal decomposition of $FeC_2O_4$ causes the endothermic peak at nearly 400℃[30] followed with the glucose carbonization at above 500℃.

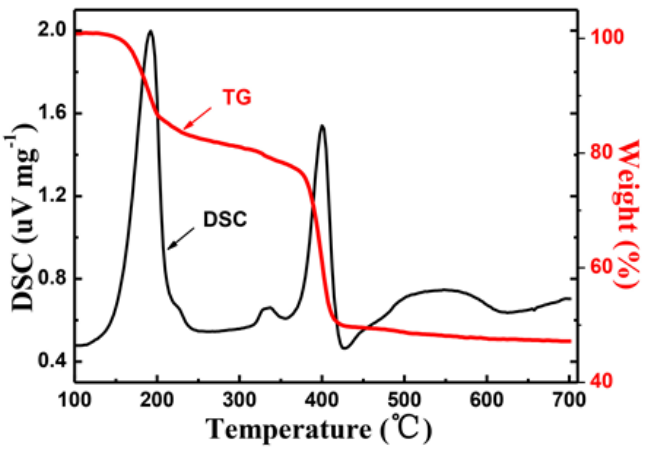


**Fig. 1** TG-DSC curve of the $FeO_x$/graphene ($m_{FOD}$:$m_{GO}$ = 100:1.5) precursor.

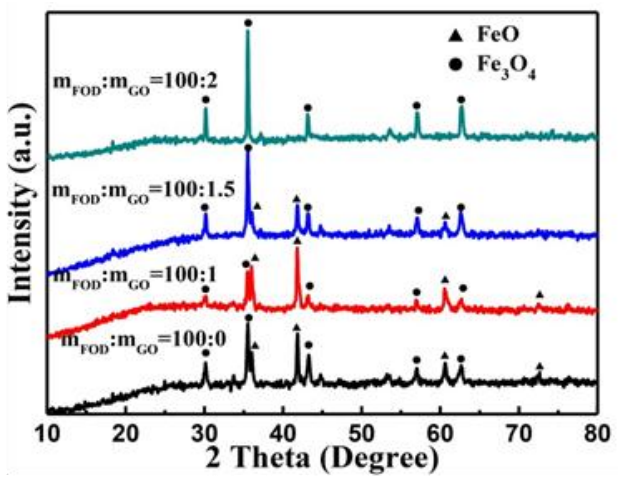


**Fig. 2** XRD patterns of $FeO_x$/graphene composites based on different weight ratios of FOD and GO.

Journal Name

RSCPublishing

ARTICLE

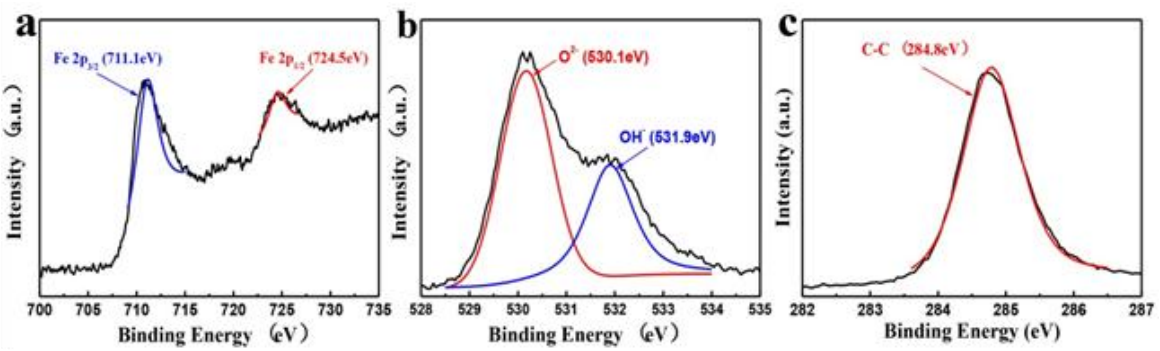


**Fig. 3** Deconvoluted Fe 2p (a), O 1s (b) and C 1s (c) XPS spectra of $FeO_x$/ graphene hybrids ($m_{FOD}$:$m_{GO}$ = 100:1.5)

Fig. 2 shows the XRD patterns of the $FeO_x$ composites based on the weight ratios of FOD and GO. The narrow sharp peaks indicate the good crystallization of the samples. It is noteworthy that the $FeO_x$ grown on the reduced GO sheet was a mixture of $Fe_3O_4$ and FeO. Particularly, for the sample ($m_{FOD}$:$m_{GO}$ = 100:2), it is obviously noted that no FeO peaks can be detected in the product, indicating that the content of FeO particles decreased with the increase of GO. It can be supposed that the FeO particles were further oxidated by the redundant water and the oxidizing agent produced along with the reduction process of GO. To make a brief conclusion, the decomposition process of the $FeC_2O_4$•$2H_2O$ can be expressed as:

$$FeC_2O_4 \cdot 2H_2O \xrightarrow{\text{decomposition}} FeO + Fe_3O_4 + CO_2 + H_2O \qquad (1)$$

To further investigate the chemical structure of the iron particles, typical XPS analysis was evaluated and the results are shown in Fig. 3. In the XPS Fe 2p spectrum (Fig. 3a), two peaks at 711.1 eV and 724.5 eV are detected, which are assigned to Fe $2p_{3/2}$ and Fe $2p_{1/2}$ binding energies. The Fe $2p_{3/2}$ electron-binding energy observed in Fig. 3a reveals that the compound $FeO_x$ contains a majority of $Fe_3O_4$. FeO was barely detected in the XPS spectrum possibly owing to the trace content and graphene covering. The deconvoluted O 1s XPS spectrum (Fig. 3b) shows two peaks at 530.1 eV and 531.9 eV, indicating the presence of $O^{2-}$ and $OH^-$, respectively. These results obviously indicate that the iron particles exist in a mixed state of iron oxides and a small amount of intermediate product FeOOH, produced during the $FeC_2O_4$•$2H_2O$ pyrolysis. The characteristic peak of graphene at 284.8 eV is shown in detail in the XPS C 1s spectrum (Fig. 3c), which confirmed the existence of reduced graphene oxide (rGO). The high temperature reaction process of $FeO_x$ recrystallization and graphene oxide reduction contributes to the intensive mixing between iron oxides and graphene.

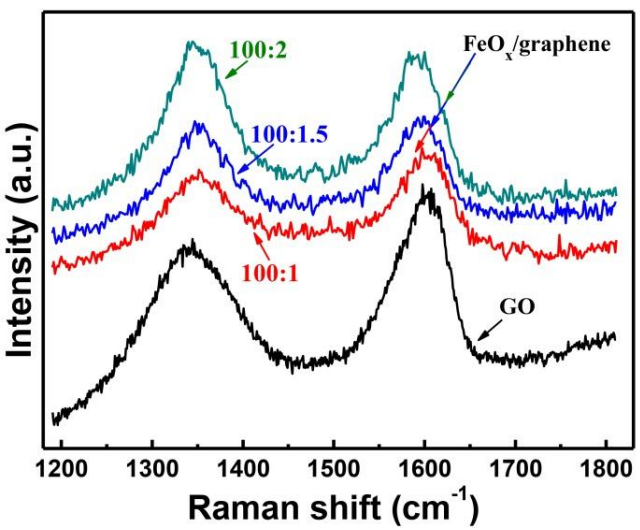


**Fig. 4** Raman spectra of graphene oxide and $FeO_x$/graphene composites based on different weight ratios of FOD and GO.

Raman spectroscopy is widely used to evaluate the reduction degree of GO. The spectra of graphene oxide and $FeO_x$/graphene composites are plotted in Fig. 4. Characteristic peaks of $FeO_x$/graphene materials at around 1340 $cm^{-1}$ (D band) and around 1590 $cm^{-1}$ (G band) are detected. The intensity ratio of D and G peak ($I_D/I_G$) reveals the disorder density of carbon materials. As shown in Fig. 4, compared with the GO ($I_D/I_G$ = 0.86), the $I_D/I_G$ of $FeO_x$/graphene is increased to nearly 1.10 due to the removal of oxygen-containing functional groups during the progress of GO reduction. The analysis of Raman spectra indicate that GO in the composite is reduced sufficiently.

SEM image of the $FeO_x$/graphene ($m_{FOD}$:$m_{GO}$ = 100:1.5) composites (Fig. 5a) reveals that the $FeO_x$ nanoparticles coat on the graphene sheet evenly. Most of the nanoparticles are sphere shape with the diameters ranging from 20 to 100 nm, compared with the blank sample (Fig. 5b), which are in the size range of 1-3 μm, and strongly aggregate together. It is because that direct growth of inorganic nanomaterials on mildly oxidized nanocarbon materials affords strong covalent coupling between inorganic nanocrystals and carbon materials[27], which impedes the nanoparticles from crystallization. In Fig. 5c, the TEM image clearly shows the nanoparticle grown on the GE sheets. The HRTEM image of the $FeO_x$/graphene composites shown in Fig. 5d reveals the lattice spacing of 0.47 nm corresponding to the (111) plane of $Fe_3O_4$ which deeply proves the existence of $Fe_3O_4$ in the $FeO_x$ composites.

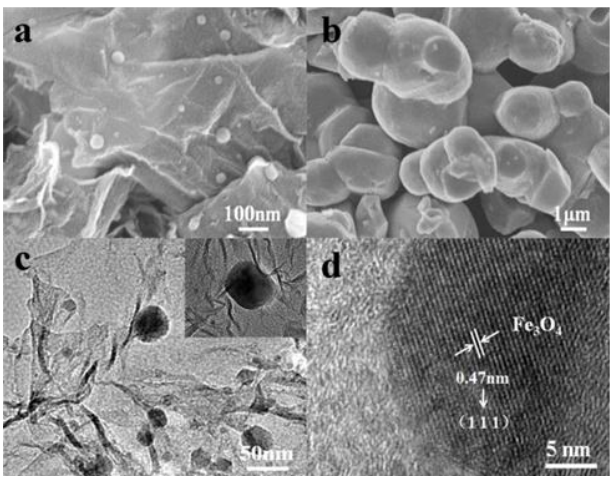


**Fig. 5** SEM images of the $FeO_x$/graphene composites, (a) $m_{FOD}$:$m_{GO}$ = 100:1.5 (b) $m_{FOD}$:$m_{GO}$ = 100:0; (c) TEM and (d) HRTEM images of the $FeO_x$/graphene ($m_{FOD}$:$m_{GO}$ = 100:1.5).

Cyclic voltammograms (CVs) have been performed to investigate the oxidation-reduction behavior of $FeO_x$/graphene system. Fig. 6a shows the CV curves of the different FeOx electrodes. The $FeO_x$/graphene ($m_{FOD}$:$m_{GO}$ = 100:1.5) sample performs a better reversible electrochemical oxidation-reduction process, relatively. Even at larger scan rates (Fig. 6b), the strong oxidation and reduction peaks are still observed implying the excellent reversibility of the hybrid materials at high current density. According to the previous study[31, 32], multiple peaks should be observed in the CV curves on the behalf of redox reaction of iron electrode. But, in particular, the CV curve only emerges one overlapping redox peak at -1.08 V, mainly involving with the conversion between $Fe^{2+}$ to Fe. Two obvious oxidation peaks at -0.87 V and -0.55 V, emerging higher potential and stronger intensity. Respectively, the two oxidation peaks represent $Fe/Fe^{2+}$ and $Fe^{2+}/Fe^{3+}$ which can be indicated by the following reactions[32]:

$$Fe+2OH^- \underset{\text{charge}}{\overset{\text{discharge}}{\rightleftharpoons}} Fe(OH)_2+2e^- \qquad E^0=-0.877V \qquad (2)$$

$$Fe(OH)_2+OH^- \underset{\text{charge}}{\overset{\text{discharge}}{\rightleftharpoons}} FeOOH+H_2O+e^- \qquad E^0=-0.560V \qquad (3)$$

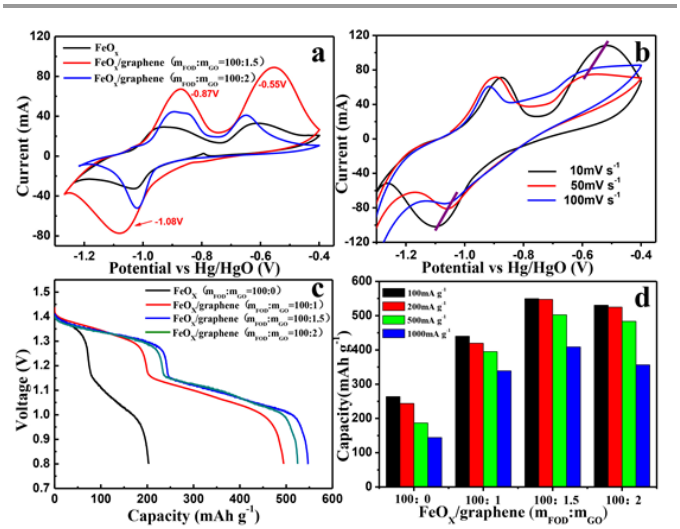


**Fig. 6** (a) CV curves of $FeO_x$/graphene hybrids ($m_{FOD}$:$m_{GO}$ = 100:0, 100:1.5, 100:2) at a scan rates of 5 mV $s^{-1}$; (b) CV curves of $FeO_x$/graphene hybrids ($m_{FOD}$:$m_{GO}$ = 100:1.5) at 10 mV $s^{-1}$, 50 mV $s^{-1}$, and 100 mV $s^{-1}$. (c) Typical discharge curves of the $FeO_x$/graphene hybrids ($m_{FOD}$:$m_{GO}$ = 100:1.5) at constant current density of 200 mA $g^{-1}$. (d) Discharge capacity of the four samples at different discharge rate (100 mA $g^{-1}$,200 mA $g^{-1}$,500 mA $g^{-1}$ and 1000 mA $g^{-1}$).

In order to investigate the specific capacity of the $FeO_x$/graphene composites, the charge-discharge cycles at a discharge current density of 200 mA $g^{-1}$ were carried out. As shown in Fig. 6c, two discharge plateaus are observed in discharge process, which can be attributed to the reaction of $Fe \rightarrow Fe^{2+}$ and $Fe^{2+} \rightarrow Fe^{3+}$, respectively. Obviously, the discharge capacities of $FeO_x$/graphene composites are more than twice as much as the blank sample. Especially for the samples ($m_{FOD}$:$m_{GO}$ = 100:1.5), the maximum discharge capacity can maintain at 552.1 mAh $g^{-1}$(compared with 222.6 mAh $g^{-1}$ of the $FeO_x$ material without graphene). The electrochemical performance of the $FeO_x$/graphene hybrids is further evaluated by high-rate discharge measurement. Fig. 6d shows the discharge capacity of the $FeO_x$/graphene hybrids at different current densities from 100 mA $g^{-1}$ to 1000 mA $g^{-1}$. As expected, our $FeO_x$/graphene composites express excellent high-rate performance. Especially for the optimal sample ($m_{FOD}$:$m_{GO}$ = 100:1.5), the specific capacity converted from 549.4 mAh $g^{-1}$ to 408.5 mAh $g^{-1}$, based on the discharge current densities of 100 mA $g^{-1}$ and 1000 mA $g^{-1}$, respectively. The outstanding electrochemical performance can be attributed to the following reasons: first of all, the size of the $FeO_x$ particles decrease to a large extent because of the strong coupling with graphene during decomposition-crystallization progress, which contributes to larger efficient surface area. Another important reason is that GE layers can enhance the electron transfer through the nano-sized active materials during charging and discharging.

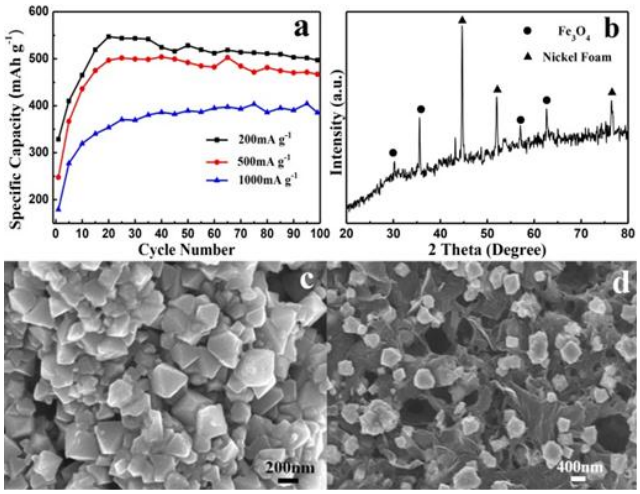


**Fig. 7** (a) Cycling performance of $FeO_x$/graphene hybrids ($m_{FOD}$:$m_{GO}$ = 100:1.5) at different discharge current density (200 mA $g^{-1}$,500 mA $g^{-1}$ and 1000 mA $g^{-1}$); (b) XRD patterns of $FeO_x$/graphene hybrids ($m_{FOD}$:$m_{GO}$ = 100:1.5) at discharge state after 100 cycles; SEM images of (c) blank sample and (d) $FeO_x$/graphene ($m_{FOD}$:$m_{GO}$ = 100:1.5) sample at charge state after 100 cycles.

Fig. 7a shows the cycle stability of the $FeO_x$/graphene composite ($m_{FOD}$:$m_{GO}$ = 100:1.5) electrode at the discharge current densities of 200 mA $g^{-1}$ to 1000 mA $g^{-1}$. About 80% of the initial capacity is maintained after 100 charge-discharge cycles at a current density of 200 mA $g^{-1}$. Additionally, even at a high discharge current density of 1000 mA $g^{-1}$, the capacity decay is still as low as 10% after 100 cycles. It is apparent that the particular electronic conductivity, salutary space effect as well as the mechanical property of GE leads to the outstanding cycle performance of the $FeO_x$/graphene electrode[27, 33, 34]. XRD pattern at discharge state (Fig. 7b) and SEM images of the two samples at charge state (Fig. 7c and Fig. 7d) were carried out to further investigate the morphology and microstructure variation of composites after 100 charge-discharge cycles. Fig. 5b shows the existence of $Fe_3O_4$ obviously, which is produced during discharge reaction. As revealed in SEM images, the reversible capacity decay is on account of the growth of iron oxide particles during cycles. Additionally, the graphene-based $FeO_x$ particles grow evenly compared with the serious aggregation of the blank $FeO_x$ particles during dissolution-deposition process. In other words, it is the highly structural stability leading to the copacetic cycle performance of $FeO_x$/graphene composites.

## 4. Conclusions

In summary, a new-style $FeO_x$ nanocomposites grown on graphene sheets were successfully synthesized via a simple high temperature solid-state reaction. The results indicated that the $FeO_x$ particles are composed of $Fe_3O_4$ and FeO with particle size around 100 nm. The $FeO_x$/graphene nanocomposites deliver an initial discharge capacity of 552.1 mAh $g^{-1}$ at current density of 200 mA $g^{-1}$. Owing to the remarkable electrochemical activity and mechanical property caused by the strong coupling between iron-oxide nanoparticles and graphene layer, the promising $FeO_x$/graphene composites exhibit enhanced high-rate capability and cycling stability. The research presented here demonstrates a simple and promising method of synthetizing iron anode materials for improving the power density of rechargeable iron battery for large-scale energy storage, as well as electric vehicles and hybrid electric vehicles.

## Acknowledgements

This study was supported by the National Nature Science Foundation of China (Grant nos. 20111061 and 21373198).

## Notes and references

Corresponding author

** Tel: 86-0431-85262447; 86-0431-85262404, Fax: 86-0431-85262836.*

*E-mail: lmwang@ciac.ac.cn; ymwu@ciac.ac.cn.*

[a] *State Key Laboratory of Rare Earth Resource Utilization, Changchun Institute of Applied Chemistry, CAS, Changchun 130022, China*

[b] *Changzhou Institute of Energy Storage Materials and Devices, Changzhou 213000, China*

[c] *Faculty of Chemistry, Northeast Normal University, Changchun 130024, China*

[d] *University of Chinese Academy of Science, Beijing 130049, China*

1. M. Armand, J.M. Tarascon, *Nature*, 2008, **451**, 652-657.
2. J.B. Goodenough, Y. Kim, *J. Power Sources*, 2011, **196**, 6688-6694.
3. F. Cheng, J. Liang, Z. Tao, *J. Chen, Adv. Mater*, 2011, **23**, 1695-1715.
4. V. Etacheri, R. Marom, R. Elazari, G. Salitra, D. Aurbach, *Energy Environ. Sci*, 2011, **4**, 3243-3262.
5. J.B. Goodenough, Y. Kim, *Chem. Mater*, 2010, **22**, 587-603.
6. P.G. Bruce, B. Scrosati, J.-M. Tarascon, *Angew. Chem., Int. Ed.*, 2008, **47** 2930-2946.
7. G. Halpert, *J. Power Sources*, 1984, **12**, 177-192.
8. A.K. Shukla, M.K. Ravikumar, T.S. Balasubramanian, *J. Power Sources*, 1994, **51**, 29-36.
9. C. Chakkaravarthy, P. Periasamy, S. Jegannathan, K.I. Vasu, *J. Power Sources*, 1991, **35**, 21-35.
10. C.A.C. Souza, I.A. Carlos, M. Lopes, G.A. Finazzi, M.R.H. de Almeida, *J. Power Sources*, 2004, **132**, 288-290.
11. A.K. Manohar, S. Malkhandi, B. Yang, C.G. Yang, G.K.S. Prakash, S.R. Narayanan, *J. Electrochem. Soc*, 2012, **159**, A1209-A1214.
12. S. Malkhandi, B.Yang, A.K. Manohar, G.K.S. Prakash, S.R. Narayanan, *J. Am. Chem. Soc.*, 2012, **135**, 347-353.
13. P. Periasamy, B.R. Babu, S.V. Iyer, *J. Power Sources*, 1996, **58**, 35-40.
14. W.C. He, H.B. Shao, Q.Q. Chen, J.M. Wang, J.Q. Mang, *Acta Phys. Chim. Sin*, 2007, **23**, 1525-1530.
15. A.K. Manohar, C.G. Yang, S. Malkhandi, B. Yang, G.K.S. Prakash, S.R. Narayanan, *J. Electrochem. Soc*, 2012, **159**, A2148-A2155.
16. X. Huang, X.Y. Qi, F. Boey, H. Zhang, *Chem. Soc. Rev*, 2012, **41**, 666-686.
17. J.H. Zhu, M.J. Chen, Q.L. He, L. Shao, S.Y. Wei, Z.H. Guo, *RSC Adv.*, 2013, **3**, 22790-22824.
18. W.H. Shi, J.X. Zhu, D.H. Sim, Y.Y. Tay, Z.Y. Lu, X.J. Zhang, H. Zhang, H.H. hng, Q. Yan, *J. Mater. Chem*, 2011, **21**, 3422-3427.
19. Y. Li, L. Tang, J. Li, *Electrochem. Commun*, 2009, **11**, 846-849.

20. Z. Yin, S. Wu, X. Zhou, X. Huang, Q. Zhang, F. Boey, H. Zhang, *Small*, 2010, **6**, 307-312.
21. H. Liu, S. Ryu, Z. Chen, M.L. Steigerwald, C. Nuckolls, L. E. Brus, *J. Am. Chem. Soc.*, 2009, **131**, 17099-17101.
22. J. Zhu, T. Zhu, X. Zhou, Y. Zhang, X.W. Lou, X. Chen, H. Chen, H. Zhang, H.H. Hng, J. Ma, Q. Yan, *Nanoscale*, 2011, **3**, 1084-1089.
23. Z.-S. Wu, W. Ren, L. Wen, L. Gao, J. Zhao, Z. Chen, G. Zhou, F. Li, H.-M. Cheng, *ACS Nano*, 2010, **4**, 3187-3194.
24. S. Yang, X. Feng, S. Ivanovici, K. Müllen, *Angew. Chem., Int. Ed.*, 2010, **49**, 8408-8411.
25. H. Wang, L. -F. Cui, Y.Yang, H. Sanchez Casalongue, J.T. Robinson, Y. Liang, Y. Cui, H. Dai, *J. Am. Chem. Soc.*, 2010, **132**, 13978-13980.
26. Q.H. Wang, L.F. Jiao, H.M. Du, Y.J. Wang, H.T. Yuan, *J. Power Sources*. 2014, **245**, 101-106.
27. H.L. Wang, Y.Y. Liang, M. Gong, Y.G. Li, W. Chang, T. Mefford, J.G. Zhou, J. Wang, T. Regier, F. Wei, H.J. Dai, *Nat. Commun*, 2012, **3**, 917-924.
28. D.C. Marcano, D.V. Kosynkin, J.M. Berlin, A. Sinitskii, Z.Z. Sun, A. Slesarev, L.B. Alemany, W. Liu, J.M. Tour, *ACS NANO*, 2010, **4**, 4806-4814.
29. C.Y. Kao, K.S. Chou. *J. Power Sources*, 2010, **195**, 2399-2404.
30. Z.D. Fang, D.J. Wang, *Chinese Journal of Inorganic Chemistry*, 2005, **21**, 1682-1686.
31. P. Periasamy, B.R. Babu, S.V. Iyer, *J. Power Sources*. 1996, **58**, 35-40.
32. K. Vijayamohanan, T.S. Balasubramanian, A.K. Shukla, *J. Power Sources*, 1991, **34**, 269-285.
33. A.M. Rafiee, J. Rafiee, Z. Wang, H.H. Song, Z.Z. Yu, N. Koratkar, *ACS Nano*, 2009, **3**, 3884-3890.
34. S.L. Chou, J.Z. Wang, M. Choucair, H.K. Liu, J.A. Stride, S.X. Dou, *Electrochem.Commun*, 2010, **12**, 303-306.

## Graphic Abstract

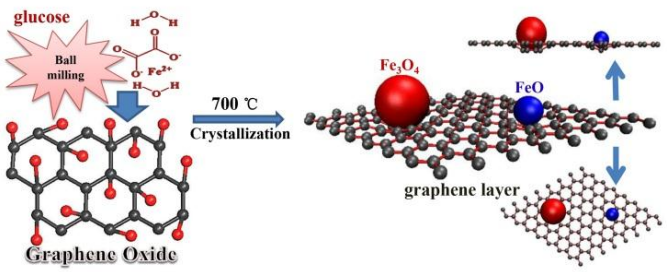

## Graphical and textual abstract

---

# Enhanced electrochemical performances of $FeO_x$/graphene hybrid as anode material for alkaline nickel-iron battery

**Wei Jiang [a, d], Fei Liang [a, b], Jianwei Wang [a, d], Lei Su [a, c], Yaoming Wu [*a, b], and Limin Wang [*a, b]**

**Keywords:** graphene-based composites; iron electrode; anode material; nickel-iron battery

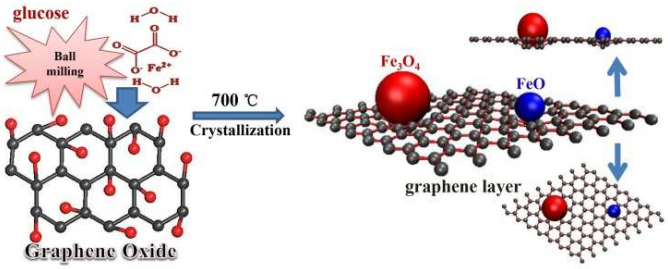


A novel hybridized $FeO_x$/graphene was synthesized by a simple high temperature solid-state reaction process instead of hydrothermal synthesis.

---

**Highlight:**

In this work, a novel hybridized $FeO_x$/graphene material was prepared through a relatively simple high temperature solid-state reaction process instead of hydrothermal synthesis.

When evaluated as anode material for alkaline nickel-iron battery, the $FeO_x$/graphene nanocomposites delivered a high specific capacity of 552.1 mAh $g^{-1}$ at current density of 200 mA $g^{-1}$ and remained 91% of the initial capacity after 100 cycles.

The $FeO_x$/graphene composites can afford excellent electrochemical performances at high discharge current density (as high as 1000 mA $g^{-1}$), aimed at applications in hybrid electric vehicles (HEV) and electric vehicles (EV) where high current response is needed.